Accumulation and partitioning of toxic trace metal(loid)s in phytoliths of wheat grown in a multi-element contaminated soil

Published in: *Environmental Pollution*

Citation for published version: Liu, L., Song, Z., Li, Q., Ellam, R.M., Tang, J., Wang, Y., Sarkar, B., Wang, H., (2022) Accumulation and partitioning of toxic trace metal(loid)s in phytoliths of wheat grown in a multi-element contaminated soil. *Environmental Pollution.* 294: 118645. doi: 10.1016/j.envpol.2021.118645.

Document version: Accepted peer-reviewed version.

Accumulation and partitioning of toxic trace metal(loid)s in phytoliths of wheat grown in a multi-element contaminated soil

Linan Liu[a,b], Zhaoliang Song[b,*], Qiang Li[b], Rob M. Ellam[c], Jingchun Tang[a], Yangyang Wang[d], Binoy Sarkar[e], Hailong Wang[f,g]

[a] College of Environmental Science and Engineering, Nankai University, Tianjin 300350, China

[b] Institute of Surface-Earth System Science, School of Earth System Science, Tianjin University, Tianjin 300072, China

[c] Scottish Universities Environmental Research Centre, East Kilbride, G750QF, Scotland, United Kingdom

[d] National Demonstration Center for Environmental and Planning, College of Environment & Planning, Henan University, Kaifeng 475004, China

[e] Lancaster Environment Centre, Lancaster University, Lancaster, LA1 4YQ, United Kingdom

[f] School of Environmental and Chemical Engineering, Foshan University, Foshan, Guangdong 528000, China

[g] Key Laboratory of Soil Contamination Bioremediation of Zhejiang Province, Zhejiang A&F University, Hangzhou, Zhejiang 311300, China

*Correspondence to: zhaoliang.song@tju.edu.cn (Song ZL)

Telephone: +86-15202264081

Address: Institute of Surface-Earth System Science, School of Earth System Science, Tianjin University, Tianjin 300072, China

Highlights

- The concentrated silica develops into various phytolith morphologies in wheat plants.
- Phytolith encapsulates metal (loid)s through their co-precipitation process in plants.
- Heavily metal-contaminated soil leads to increased TTM accumulation in phytoliths.
- PhytTMs affect long-term TTM cycles of the cropland with multi-metal contamination.

Graphical abstract

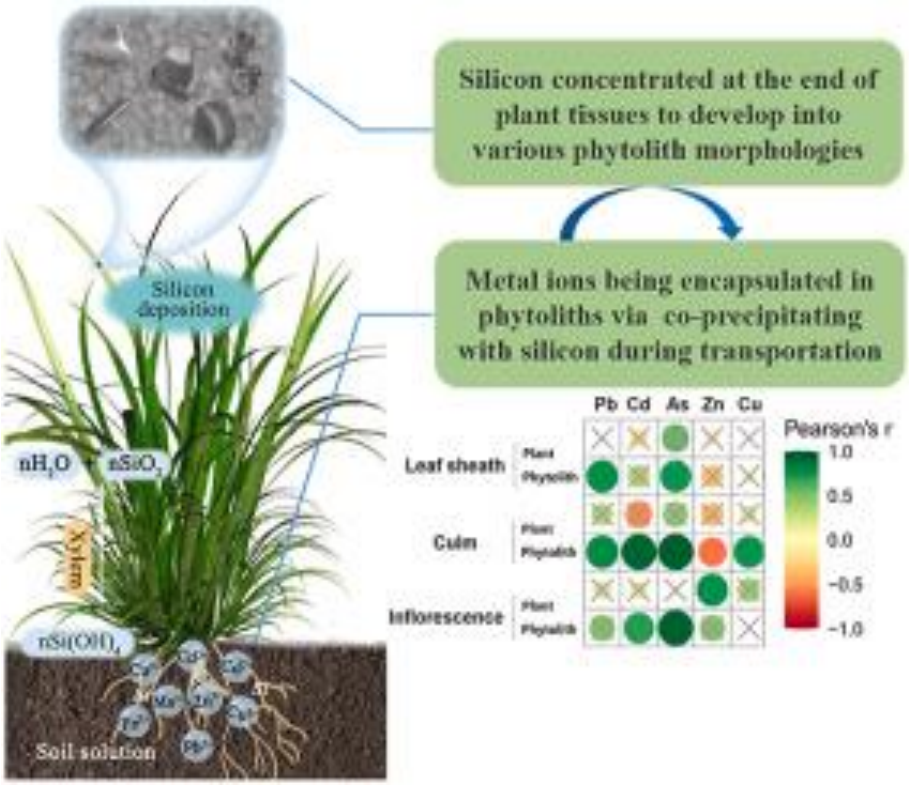

Abstract: Cropland contamination by toxic trace metal(loid)s (TTMs) has attracted increasing attention due to the serious consequential threat to crop quality and human health. Mitigation of plant TTM stress by silica amendment has been proposed recently. However, the relationship between the siliceous structure of phytoliths and TTMs in plants, and the environmental implications of phytolith-occluded trace metal(loid)s (PhytTMs) remain unclear. This study assessed the accumulation of five metal(loid)s, including lead (Pb), zinc (Zn), cadmium (Cd), copper (Cu) and arsenic (As), in the organic tissues and phytoliths of wheat grown in a mixed-TTM contaminated soil under both lightly and heavily contaminated conditions. The results show that the concentrations of plant TTMs and PhytTMs were significantly ($p < 0.05$) positively correlated, and higher in heavily contaminated wheats than those in lightly contaminated ones. The bio-enrichment factors between phytoliths and organic tissues were higher for As (1.83), Pb (0.27) and Zn (0.30) than for Cd (0.03) and Cu (0.14), implying that As, Pb and Zn were more readily co-precipitated with silicon (Si) in phytolith structures than Cd and Cu. Network analysis of the relationship between soil and plant elements with PhytTMs showed that severe contamination could impact the homeostasis of elements in plants by altering the translocation of TTMs between soils, plants, and phytoliths. The accumulation of TTMs in phytoliths was affected by the capacity of Si deposition in tissues and chelation of TTMs with silica, which could impact the role of PhytTMs in global biogeochemical TTM cycles.

Keywords: Phytolith; Toxic trace metal(loid)s; Biological enrichment; Wheat; Silicon

1. Introduction

With rising global population and development of modern industries, cropland soils are increasingly being exposed to wastewater and metal(loid)-containing waste materials including sewage, biosolids and municipal solid wastes, leading to serious contamination with toxic trace metal(loid)s (TTMs) (Soltanian et al., 2015; Wang et al., 2020a). Most soils near mining areas and smelting factories are contaminated with excessive input of TTMs, including lead (Pb), zinc (Zn), cadmium (Cd), copper (Cu), arsenic (As) and chromium (Cr), through atmospheric deposition and/or wastewater discharge (Zhou et al., 2018; Cao et al., 2021). The accumulation of TTMs reduces crop growth by hindering nutrient utilization, decreasing photosynthesis, and inducing oxidative damage to plant tissues (Abbas et al., 2018; Murtaza et al., 2019). The TTM accumulation in edible plant parts poses risks to animals and human beings through food chain transfer, and can cause various human diseases including cancer (Xue et al., 2019; Li et al., 2020), calling for extensive research to understand the contamination process and plausible mitigation strategies (Khan et al., 2020).

The role of silicon (Si) in regulating plant growth under TTM-stressed condition has recently been investigated (Adrees et al., 2015; Puppe and Sommer, 2018; Ali et al., 2019; Wang et al., 2020b). Silicon can chelate with TTMs to compartmentalize free metal(loid) ions in plant cell walls or inactive metabolic parts such as phytoliths, reducing the bioavailability of the toxic elements (Liang et al., 2005; Greger et al., 2016). For example, Rogalla and Römheld (2002) found that sodium silicate addition in the hydroponic growth medium of *Cucumber sativus* L. alleviated manganese (Mn) toxicity to the plants. The main reason was that most (> 90%) of the total Mn in leaves was bound to cell walls, thereby decreasing Mn availability to the metabolically active plant tissues through entry into the symplasmic pool. Similarly,

Si addition in cultivated cell lines of rice increased Si accumulation in the cell wall as organosilicon compounds, inducing increased Cd^{2+} co-precipitation with Si to form Si-cell wall complexes, which inhibited Cd uptake into rice cells at low Cd concentration (5 μM) (Liu et al., 2013). However, at high Cd concentration (60 μM), no significant reduction of Cd^{2+} uptake was observed in cells regardless of the Si addition rates, suggesting saturation of binding or adsorption sites for Cd^{2+} in the plant cell wall (Liu et al., 2013). Nevertheless, more research is needed to understand the roles of Si in regulating TTM distribution in plant tissues and alleviating the toxicity to plants via binding or co-precipitation with free TTM ions.

Most of the Si in plant tissues is deposited on plant cell walls/lumens or in the inter-/extra-cellular matrix, and converted eventually into phytolith structures (Ma 2010; Puppe and Sommer, 2018). During the process of silica deposition and phytolith formation, many elements, both major (e.g., C, Al, and Fe) and trace (e.g., Pb, As, Zn, and Cu), are encapsulated into phytoliths, reflecting the crucial role of phytoliths in regulating the biogeochemical cycle of these elements (Wüst and Bustin, 2003; Anala and Nambisan, 2015; Song et al., 2016; Tran et al., 2019; Delplace et al., 2020). In the last decade, many studies have reported that Si plays an important role in long-term C sequestration through the production of phytolith-occluded C (PhytOC), which further affects the global C cycle, and hence, climate change (Song et al., 2013; Qi et al., 2017; Zhang et al., 2020). Therefore, TTMs such as Pb, Cu, As, Mn and Zn could also be sequestrated within phytoliths, thereby constituting an overlooked pool of TTMs in contaminated soil-plant system (Nguyen et al., 2019; 2021; Tran et al., 2019; Delplace et al., 2020). However, the effects of phytolith-occluded trace metal(loid)s (PhytTMs) on the long-term biogeochemical cycles of these elements, their phytolith-mediated detoxification mechanisms inside plant bodies, and the response of PhytTMs to

environmental changes are unclear. Various Si uptake and accumulation patterns across plant species lead to formation of distinctive amounts of phytoliths and PhytTMs in different species and types of tissues (Ma and Yamaji, 2008; Song et al., 2014; Guerriero et al., 2020). In addition, phytolith stability is impacted by the specific surface structures and organic matter composition of phytoliths, as well as environmental conditions (e.g., temperature and soil pH), which in turn would affect the sequestration or re-cycling of PhytTMs, especially for Si-accumulating plants (Li et al., 2014; Trinh et al., 2017; Nguyen et al., 2019).

Wheat (*Triticum aestivum* L.) is a Si-accumulator, and also one of the globally most important food crops with cultivated areas accounting for ~20% of the world arable lands (Pan, 2014; Yang et al., 2019). Investigation on the effects of Si for PhytTM formation in wheat plants and studying factors influencing the TTM sequestration by phytolith structures could provide new perspectives to understand the long-term biogeochemical cycling of PhytTMs in croplands with mixed-contaminated conditions (Delplace et al., 2020; Nguyen et al., 2021). The present study aims to investigate the role of Si in TTM translocation and PhytTM production in wheat tissues by comparing lightly and heavily contaminated soil conditions. We hypothesize that: i) TTMs could be co-precipitated with silica and accumulated in phytolith structures, decreasing TTM bioavailability in plant tissues; and ii) severe TTM contamination in the soil could disturb elemental homeostasis in plant tissues, leading to alteration of TTM transportation and accumulation in plant organic tissues and phytolith structures that are associated with PhytTM production. We further explore the mechanisms underlying TTM detoxification in plants via interaction with silica in tissues. This study provides a new insight into the sequestration and release kinetics of TTM in/from PhytTMs, which enables better understanding of the effects

of PhytTM on regulating biogeochemical TTM cycling.

2. Materials and methods

2.1 Study site and sampling strategy

The study site is an area of cropland soils affected by multi-TTM contamination from an adjacent non-ferrous Pb/Zn smelter in Jiaozuo, Henan Province, China (Fig. S1). This region is favorable for growing crops with a mild climate, ample sunshine and rainfall. The average annual temperature is 14.4°C with a maximum temperature (28°C) in July, and a minimum temperature (-2°C) in January. The average annual precipitation is 584 mm with most rainfall occurring in the summer. Prevailing winds are northeasterly, and the annual mean wind speed is 2.9 m s^{-1}. In addition to TTM-containing minerals originating from the smelter, croplands in the sampling area receive industrial sewage discharges and exhaust gas emissions. Wang et al. (2019b) reported that concentrations of Cd, Pb, Cr and Zn in the farmland region surrounding the Pb/Zn smelter were respectively 23.0, 2.2, 1.5 and 1.1 times higher than background soil concentrations in the Henan Province.

Paired winter wheat plants and soil samples were collected when plants attained physiological maturity in early June 2018. Previous assessment of TTM spatial distribution in the farmland established that severely polluted soils were found closer to the smelter (Wang et al., 2019b). As the prevailing wind is northeasterly, sampling sites downwind (southwestern) of the smelter are most contaminated while those to the southeast of the smelter are less contaminated. Therefore, we selected lightly polluted samples (LPs) and heavily polluted samples (HPs) according to their distance from the smelter and relationship to the prevailing wind (Fig. S1). For each transect, eight (3 m × 3 m) sampling plots were arranged roughly radial to the central location

of the smelter. The first plot, closest to the smelter, was arbitrarily fixed as the origin of the pollution source (i.e., 0 m), and the other seven plots were 5 m, 10 m, 20 m, 40 m, 70 m, 110 m and 160 m away from that origin (Fig. S1). At each plot, three regularly-spaced sites were selected randomly and approximately 13~17 wheats were collected in each site, and the samples from all three sub-sites (i.e., approximately 45) were aggregated into single mixed plant samples. Topsoil (0~20 cm) samples were collected using a cutting ring method, and each sample was composed of three sub-samples from the same plot. Each of the mixed samples was packed individually in ziplock bags and taken to the laboratory for analysis.

2.2 Sample processing and analysis

2.2.1 Soil samples

After removal of visible plant remains and stones, soil samples were air-dried, and crushed to < 2 mm particles for further analysis. Measurements of soil pH and electrical conductivity (EC) were conducted in a 1:2.5 suspension (i.e., 10 g soil in 25 g deionized water). Soil bulk density was measured using a cutting ring method based on the weight of air-dried soil per volume sample. Soil moisture content was measured gravimetrically based on the comparative weight of fresh and oven-dried samples. Soil particle fractions were analyzed using an Ultra-High-Speed Intelligent Particle Size Analyzer (Malvern Mastersizer 3000, England), and classified into clay (0.01~2 μm), silt (2~200 μm) and sand (200~2000 μm) fractions (Bai et al., 2017).

The soil samples were homogenized by cone and quartering, then ground to < 0.15 mm using an agate mortar for elemental analysis. Soil organic carbon (SOC) content was determined using potassium dichromate wet-oxidation combined with a spectrophotometric method (Walkley and Black, 1934). Available nitrogen (N) was

measured using an alkaline-hydrolysis diffusion method (Bao, 2000). Available phosphorus (P) was determined using a colorimetric molybdate blue method (Zhao and Zeng, 2019). Contents of total TTMs in the soil samples after digestion with a HNO_3, HCl and HF mixture (6:2:1) were measured using an inductively coupled plasma mass spectrometer (ICP-MS 7900, Agilent, USA). The bioavailable contents (extractable in 0.01 mol L^{-1} calcium chloride ($CaCl_2$)) of Si (Hogan et al., 2018) and TTMs (Zhou et al., 2018) in the soil were determined by colorimetric and ICP-MS methods, respectively.

2.2.2 Plant samples

Above-ground plant samples were separated into inflorescence, leaf sheath and culms, ultrasonicated and washed with deionized water to remove impurities, and oven-dried at 70°C for about 24 h to a constant weight. Each above-ground plant part was divided equally into two aliquots, one of which was ground into powder using a micro grinding machine. Total contents of Si and P in plants were determined using a UV spectrophotometer (UV-1800, Shimadzu, Japan) following the molybdenum blue colorimetric method at different wavelength after digestion with Li-metaborate at 950°C for 30 min (Lu, 2000). Total C and N contents were measured using an Elementar Vario EL III elemental analyzer (Elementar Analysensysteme, GmnH, Germany). Total contents of TTMs, including Pb, Zn, Cu, Cd and As, in plants were determined by ICP-MS using a method modified from Tan et al. (2020) after digestion with "inverse" *aqua regia* (3:1 HNO_3: HCl) using a microwave digestion system (Mar6 Classic, CEM, USA), at 180°C for 25 min.

2.3 Phytolith extraction and characterization

The second aliquots of the above-ground plant samples were cut into 2-mm pieces for phytolith extraction according to a wet oxidation method modified after that described by Liu et al. (2020a), to obtain high amount of phytoliths by adding increased number of individual plants in the aliquot. Briefly, 2.5 g of dried plant fragments were digested in a 50 mL glass digestion tank with 25 mL concentrated HNO_3 and 5 mL 30% H_2O_2. Samples in triplicate were placed in a temperature-controlled graphite digestion apparatus (DigiBlock ED54, LabTech, China) for 4 h at 150°C. After digestion, potassium dichromate and concentrated sulfuric acid were added to oxidize completely the organic matter surrounding the phytoliths, then rinsed until all residual reagents were removed. The pure phytolith samples were dried and weighed, then gently powdered in an agate mortar and stored for elemental analysis. The morphological structure and the elemental composition of the phytoliths in wheat tissues were assessed using a field emission scanning electron microscope (FE-SEM) equipped with an energy dispersive X-ray spectrometer (EDS) (FE-SEM Sigma 500, Zeiss, Germany). A digestion method similar to the soil analysis was also used to digest the phytolith samples, and total TTM contents in phytoliths were measured by ICP-MS. PhytTM concentrations in plant tissues are reported as the amount of PhytTMs in unit weight of the tissue biomass.

2.4 Statistical analysis

All data are presented as the mean values of three replicates, and differences between contamination levels and wheat tissues were analyzed using one-way ANOVA and Independent-Sample Test with SPSS 17.0 software. Pearson correlation coefficients were calculated to evaluate the strength of relationship between soil properties, and displayed with a heatmap plotted using R software. Principal

component analysis (PCA) was used to create indices and reduce collinearity between multiple variables based on a correlation matrix with Origin 2018b. Relationships between plant TTMs and PhytTMs were determined using linear regression analysis, and correlations were determined using a Pearson's bivariate correlation analysis with a two-tailed t-test. Enrichment factors were calculated as the ratio of TTM contents in plant tissues and in soils ($EF_{plant\text{-}soil}$), and TTM contents in phytoliths and in plant tissues ($EF_{phytolith\text{-}plant}$), in order to assess the distribution and accumulation of TTMs in soil-plant and plant-phytolith systems (Delplace et al., 2020). Networks between elements in soils and plants, and PhytTMs were visualized by using the Pearson correlation matrix to analyze the impact factors for PhytTMs from soils and plants.

3. Results

3.1 Soil properties and toxic trace metal(loid)s

Soil physicochemical properties including nutrient and TTM contents are shown in Table 1. Soil pH was significantly higher in LP soils than HP soils. Clay and silt fractions (> 80%) constituted the main soil texture, showing significantly higher values in LP soils than HP soils. The SOC and available Si contents were also significantly higher in LP soils than HP soils. However, soil available N and P contents showed no significant difference ($p > 0.05$) between differently polluted soils.

Almost all of the total and available TTM contents, except for As, were dramatically higher in HP soils than those in LP soils. Total Pb content showed the highest value compared with other TTMs, while available Pb content showed the lowest value among measured TTMs. In contrast, total Cd content showed the lowest value among all of the total TTMs, while available Cd content was the highest among

the available TTMs. The contents of total Cd, Pb and Zn in HP soils were respectively 4.0, 2.6 and 1.8 times higher than those in LP soils, and the contents of available Cd, Pb and Zn in HP soils were respectively 5.7, 5.5 and 3.6 times higher than those in LP soils. Total As content in HP soils was almost 1.7 times higher than that in LP soils. However, available As content showed no significant differences ($p > 0.05$) between differently polluted soils.

3.2 Silicon content and phytolith characterization in wheat tissues

The Si content differed significantly between wheat tissues, showing the highest level in inflorescence (3.61 to 5.78%) followed by leaf sheath (2.83 to 5.12%), which were much higher than those in culm (1.20 to 2.30%). Although Si contents in wheat tissues were higher in LPs than HPs, no significant difference ($p > 0.05$) was found in individual tissue type between LPs and HPs (Table 2). A similar decreasing trend of phytolith content was found in wheat tissues in the order: inflorescence (10.50 ± 1.57%) > leaf sheath (9.49 ± 1.55%) > culm (3.69 ± 0.72%). Meanwhile, a significantly higher phytolith content was found in LPs than that in HPs for wheat inflorescence (Table 2).

According to the FE-SEM-EDS observations (Figs. 1 and S2), phytoliths were assembled as nano-silica particles giving various types of phytolith morphologies depending on plant tissue types. Long dendritic phytoliths (≈ 100 μm) (Figs. 1a and 1c) were mainly produced in the inflorescence tissue, while short cell phytoliths including silicified stomatal cell, rondel and hat-shaped phytoliths were produced in leaf sheath and culm tissues (Figs. 1f, 1h, 1j, 1l). There were also silicified epidermal long cells characterized by sinuous edges or elongate smooth edges in the culm tissue (Figs. 1i and 1k). In addition, phytoliths with similar morphologies in the same tissues

under the two soil pollution conditions showed variable size of nano-silica, smoothness, and compactness of phytolith surfaces (Figs. 1A and 1C, 1B and 1D, 1F and 1H).

3.3 Toxic trace metal(loid) contents in wheat tissues and phytoliths

The contents of Pb, Zn, Cd, Cu and As were determined to compare the difference of TTM distribution in plant tissues and phytoliths of wheat under different pollution conditions (Fig. 2 and Table S1). Most TTMs in plant tissues and phytoliths were significantly higher in HPs than in LPs (Fig. 2). TTM contents were significantly different between wheat tissues, and the highest TTM was observed in leaf sheaths (Table S1). The lowest contents of Pb and Zn were found in culms, while other TTMs (i.e., Cd, Cu and As) were the lowest in inflorescence. The contents of TTMs in phytoliths showed different relative abundances to those in the organic tissues. The highest contents of Pb and Cd in leaf phytoliths were more than twice higher than those in inflorescence phytoliths. However, Cu content showed an opposite trend, being about twice higher in culm and inflorescence phytoliths than that in leaf phytoliths. The highest As content was in culm phytoliths, while the lowest content of As was found in inflorescence phytoliths of LPs and leaf phytoliths of HPs. Zn contents in phytoliths also showed differences between LPs and HPs. In LPs, the highest Zn content in leaf phytoliths was about 1.5 and 2.0 times higher than that in inflorescence and culm phytoliths, respectively. In HPs, the highest Zn content in culm phytoliths was about 1.5 and 2.0 times higher than that in leaf and inflorescence phytoliths.

The contents of Pb, Zn, Cd and Cu in plant tissues showed significantly positive correlation with those of PhytPb, PhytZn, PhytCd and PhytCu, respectively, in HPs

(Table 3). However, the content of As in culm and inflorescence tissues was not significantly (p > 0.05) correlated with that of PhytAs in HPs. Additionally, the contents of PhytTMs for all TTMs differed significantly between wheat tissues, and were higher in HPs than in LPs (Table S1). The PhytTM contents, except for Cu, were higher in leaf sheaths than in culms and inflorescences. The highest PhytCu content in inflorescences was more than twice of that in leaf sheaths and culms.

3.4 Enrichment factors of toxic trace metal(loid)s in plants and phytoliths

Enrichment factors (EFs) of TTMs in different wheat tissues between plant-soil ($EF_{plant\text{-}soil}$) and phytolith-plant systems ($EF_{phytolith\text{-}plant}$) were calculated to assess the capacity of TTM transportation from soil to plants, and from plant organic tissues to their corresponding phytoliths (Fig. 3). Results showed that the values of $EF_{plant\text{-}soil}$ for all TTMs were higher in leaf sheaths than those in culms and inflorescences (Figs. 3a-3c). Furthermore, the $EF_{plant\text{-}soil}$ values of Zn, Cd and Cu were much higher than those of As and Pb. In addition, the $EF_{plant\text{-}soil}$ of Pb, Zn, Cd and As in inflorescences showed significantly higher values in LPs than those in HPs, while the $EF_{plant\text{-}soil}$ of Cu in leaf sheaths was significantly higher in HPs than in LPs.

The differences in $EF_{phytolith\text{-}plant}$ results among TTMs and tissue types showed an inconsistent trend as opposed to $EF_{plant\text{-}soil}$ results (Figs. 3d-3f). The $EF_{phytolith\text{-}plant}$ of As was higher than other TTMs in each tissue type, in the order: culms (2.52) > inflorescences (2.02) > leaf sheaths (0.93). The $EF_{phytolith\text{-}plant}$ of Cd and Cu were lower than other TTMs in each tissue type, in the order: inflorescences > culms > leaf sheaths. The highest $EF_{phytolith\text{-}plant}$ of Pb and Zn were in culms, while their lowest $EF_{phytolith\text{-}plant}$ were in leaf sheaths and inflorescences, respectively. There was a significantly higher $EF_{phytolith\text{-}plant}$ of As in LPs than in HPs for leaf sheaths, but a

significantly lower $EF_{phytolith\text{-}plant}$ of As in LPs than in HPs for inflorescences. The $EF_{phytolith\text{-}plant}$ of Zn and Cu in culms, and Cu in inflorescences were significantly higher in HPs than those in LPs.

4. Discussion

4.1 Effect of soil properties on TTM bioavailability

Excessive discharge of TTMs can increase the total content of TTMs in soils and the bioavailability of TTMs to plants (Zheng et al., 2020). In the present study, a principal component analysis (PCA) for the whole data set of soil properties is able to distinguish between the two regimes of pollution conditions (HPs and LPs) (Fig. 4). The first two principal components account for more than 60% of the total variation. The rotation load matrix of the first principal component shows that the largest loading was TTM content, especially Pb, Zn and Cd. These results demonstrate that TTMs from atmospheric deposition and/or point-source discharge play crucial roles in building up the contamination in HPs (Borůvka et al., 2005; Wang et al., 2019a). In the second principal component, soil available P, water content and clay/silt fractions show higher loading than other soil parameters, indicating that cropland management practices (e.g., fertilization and irrigation) and soil developmental stage play key roles in building up the contamination in LPs.

A close association of TTMs with soil pH, SOC content and available Si is found based on their notably more negative correlations with soil TTMs than for other soil parameters (Mao et al., 2019; Zheng et al., 2020) (Figs. 4 and S3). Ata-Ul-Karim et al. (2020) suggested that soil pH and soil organic matter were the two most crucial factors in regulating TTM transportation and bioavailability. They found that lower Cd phytoavailability in the soil-plant system was characteristic of higher soil pH

conditions due to the increase of metal-ion hydrolysis and binding sites for Cd^{2+} in soil solid phases (Loganathan et al., 2012; Alam et al., 2020; Ata-Ul-Karim et al., 2020; Zheng et al., 2020). In addition, an increase of soil bioavailable Si can inhibit TTM transportation from soil to plant shoots through increasing pH in the rhizosphere (Liang et al., 2005; Adrees et al., 2015). For example, potassium silicate addition in pot-cultivated rice significantly increased soil pH compared to the control, leading to an increase of Cd^{2+} retention in plant roots and reduction of Cd transportation from roots to shoots (Cai et al., 2020). Furthermore, Si accumulation in wheat plants could act as an apoplastic barrier to decrease the mobility of TTM ions by isolating TTM in the metabolically inactive parts of plant tissues (Rizwan et al., 2012). In the present study, soil available Si is positively correlated with soil pH but negatively correlated with soil TTMs (both total and $CaCl_2$-extractable TTMs), demonstrating that increase of soil pH and/or bioavailable Si is a promising strategy to decrease the bioavailability of TTMs in plants (Yin et al., 2016; Wang et al., 2021). However, a better understanding of the interaction between bioavailable Si content, and rhizosphere soil conditions, nutrient utilization and TTM translocation in the soil-plant system is needed to assess the benefits for contaminated-soil remediation by using Si-rich amendments in croplands (Huang et al., 2019).

4.2 Comparison of TTM accumulation in organic tissues and phytoliths

Because the transportation of TTMs in soil-plant and plant-phytolith systems depends on metal speciation and plant genotypes, we use enrichment factor ($EF_{plant\text{-}soil}$ and $EF_{phytolith\text{-}plant}$) as a uniform indicator of TTM accumulation capacity in plant tissues and phytolith structures (Wüst and Bustin, 2003; Ata-Ul-Karim et al., 2020). In this study, despite the highly polluted nature of the experimental soil, $EF_{plant\text{-}soil}$

values for TTMs were < 1, indicating a tolerance of wheat to TTM stress, or a high accumulation of Si in plants to compartmentalize TTM in roots (Murtaza et al., 2019; Delplace et al., 2020). Higher $EF_{plant\text{-}soil}$ was observed for Zn, Cd and Cu compared to Pb and As, indicating that the former three elements were more readily taken up by plants from the soil than the latter two elements, which is consistent with previous reports (Wang et al., 2016; Castaldi et al., 2018; Liu et al., 2020b). The variation of $EF_{phytolith\text{-}plant}$ between TTMs was different from that of $EF_{plant\text{-}soil}$ (Fig. 3). Although Zn, Cu and Cd were readily transported to plant aerial parts with high values of $EF_{plant\text{-}soil}$, their $EF_{phytolith\text{-}plant}$ values were lower than Pb and As. Therefore, high mobility of TTM might decrease their co-precipitation by silica during transportation within plant tissues. In contrast, despite Pb and As showed limited uptake and transport to the aerial parts of wheat plants with low $EF_{plant\text{-}soil}$ values, their $EF_{phytolith\text{-}plant}$ were higher than Cu and Cd, indicating that Pb and As might have been significantly occluded within phytoliths (Delplace et al., 2020).

Toxic trace metal(loid)s could be co-precipitated with silica, leading to their long-term sequestration in phytoliths. Silicon accumulation in plant tissues could bind TTM ions in cell walls due to increased adsorption sites, or sequestrate TTM in epidermic cells via co-precipitation with silica, which could decrease the mobility and availability of TTM, and hence alleviate TTM toxicity to plants (Adrees et al. 2015; Imtiaz et al. 2016; Cui et al., 2017; Ma et al., 2017; Liu et al., 2020b). Some TTMs such as Pb, Zn, As, Cu and Mn could be accumulated in the phytoliths of plant shoots, forming a potential PhytTM pool in the soil-plant system (Nguyen et al., 2019; Delplace et al., 2020). However, TTM translocation in organic tissues and phytoliths under altered soil environmental conditions as affected by Si uptake in different plant species and tissue types is not fully understood, which warrants future studies. The

present study contrasts TTM contents sequestrated in the phytoliths of different wheat tissues under HP and LP conditions and finds that more TTMs can be accumulated in phytoliths under higher contamination conditions (Fig. 2).

Higher content of TTMs was observed in wheat leaves than culms and inflorescences, whereas higher content of Cu and As in phytoliths was observed in culms than leaves (Table S1). Meanwhile, the lower $EF_{phytolith\text{-}plant}$ value of As in phytoliths of wheat leaves and culms under HPs than LPs might result from a specific interaction between As and Si, showing a strong protection mechanism of Si against As uptake in plants under heavily TTM-stressed conditions. These observations imply dissimilar transportation mechanisms of TTMs from organic tissues to phytolith structures, depending on TTM speciation, which might be associated with complexation and competition reactions between silica and TTM ions during transportation within plants. Therefore, it is of great significance to investigate the responses of various TTMs to Si accumulation under TTM stressed conditions, and thorough investigation is necessary to recognize the role of PhytTMs in alleviating TTM toxicity to plants and regulating the long-term TTM cycles in croplands.

4.3 Mechanism of PhytTM formation as influenced by environmental factors

Silicon is transported to plant shoots along with transpirational volume via xylem after being taken up by roots from soil solutions in the form of $Si(OH)_4$. It is then deposited in plant tissues where the polymerized silica eventually develops into phytoliths of various morphologies with occluded organic matter and/or inorganic elements (Parr and Sullivan., 2011; Rizwan et al., 2012; Li et al., 2017). Generally, higher amounts of amorphous silica are deposited in plant aerial tissues such as leaves or inflorescences than in roots (Nawaz et al., 2019; Paolicchi et al., 2019), indicating

that the incorporation of elements (e.g., Al, Fe, Mn) in phytoliths could be associated with the availability of those elements and the evapotranspiration rate of plants (Wüst and Bustin, 2003). Nonetheless, though overlooked in previous studies (Wang et al., 2016), environmental changes may exert controls on Si and TTM uptake and distribution in plant tissues, and influence the incorporation of TTMs into phytolith structures during the transportation of Si and metal(loid) ions in plants. Therefore, this study focuses on the sequestration of TTMs by phytoliths in the aboveground parts of wheat grown in the differentially TTM-contaminated field.

A synthetic network analysis indicates that most of the relationships between paired factors showed a stronger correlation in HPs than in LPs (Fig. 5). For example, wheat leaves showed higher positive correlation coefficients between soil bioavailable Pb and plant Cd and As in HPs than in LPs. Stronger positive correlations are found between soil bioavailable Pb with PhytCd in wheat culms and inflorescences in HPs than in LPs. These results suggest that excessive accumulation of TTMs (e.g., Pb and Cd) in soils altered element distribution and ion homeostasis in plant tissues by increasing transportation of TTM into plant shoots and their accumulation in phytoliths. Furthermore, a strongly negative correlation between plant C content and phytoliths in wheat leaves under HPs suggests a defense trade-off strategy of Si substitution for C-based structural compounds in plant tissues under severe contamination scenario (Neu et al., 2017). It was suggested that high Si accumulation in plant tissues could readily biosynthesize structural components in plant cell walls with low energy cost than C-based compounds (i.e., lignin or phenolics), which might increase TTM sequestration in phytoliths (Ma et al., 2015) and lead to high biomass C accumulation, especially for Si-accumulator plants under environmental stresses (Schaller et al., 2012; Liu et al., 2020a).

Previous research demonstrated that TTMs could be adsorbed by Si-rich biochar due to enhanced TTM adsorption sites provided by inorganic carbonates in biochar or via inner-sphere complexation with organic functional groups on biochar silicates, which might be similar to the formation of C-bound TTMs in phytolith carbon skeleton (Li et al., 2019; Nguyen et al., 2019). In addition, different transpiration sites in plant tissues could contribute to the silica precipitation process forming phytoliths of different shapes and morphologies in different tissues, which could impact the elemental composition of phytoliths (Li et al., 2014). In this study, TTM contents in culm phytoliths are generally higher than leaf and inflorescence phytoliths, which is similar to the results of Li et al. (2013) where C content is higher in stem phytoliths than sheath and leaf phytoliths. Furthermore, the capacity of phytoliths to capture organic matter and inorganic elements could be influenced by the morphological structure of phytoliths, such as their shapes, porosity and specific surface area, via physical adsorption or chemical ion exchange reaction (Li et al., 2014; Meharg and Meharg, 2015). Phytoliths might contain pores of various sizes which could fix organic and inorganic substances through diffusion (Trinh et al., 2017; Nguyen et al., 2019). Future studies are warranted to unravel the relationship between phytolith morphological characteristics and their TTM sequestration capacities using quantitative analysis techniques.

4.4 Implications of PhytTMs in biogeochemical cycling of TTMs

Phytoliths can be transferred into soils or sediments after plant withering or dying, and preserved for hundreds to thousands of years (Song et al., 2013; 2016). Due to protection by the resistant silica structure, elements occluded by phytoliths are not readily released into the environment, thereby reducing some nutrient and

essential element loss (Wüst and Bustin 2003). Therefore, the cycling of phytolith-occluded elements could influence the availability of elemental components to the process of vegetation succession, indicating their important roles in paleoclimate and paleogeology research (Wüst and Bustin, 2003). Recently, Nguyen et al. (2019) found that when phytoliths are recycled in soils after grain harvesting or during open burning of rice straw in the field, PhytPb could also be released to soils following phytolith dissolution, providing a potential source of bioavailable Pb to crop plants. In addition, the commonly applied tissues of biomass used as soil amendments could impact the release kinetics of phytolith-occluded elements because the content of phytolith-occluded matter and solubility of phytolith vary between plant tissue types (Li et al., 2014; Li and Delvaux, 2019). Since TTMs could be readily occluded in plant phytoliths, potential pollution by PhytTMs should not be overlooked. Especially, when using biomass straw of Si-accumulating plants to amend croplands, the effect of phytoliths on nutrient and TTM re-cycling should be considered carefully because phytolith stability is highly dependent on plant tissue types and soil conditions.

5. Conclusions

This study demonstrates that wheat could be considered as a TTM tolerant plant with a relatively low TTM bio-enrichment factor under mixed-contaminated soil conditions. Bioavailable As and Cd were higher in the soil than Pb, Zn and Cu, but a lower quantity of As and Cd were accumulated in the plant aerial tissues than the latter TTMs. One slight difference in the TTMs stored in wheat phytoliths from that in organic tissues is that As, Zn and Pb are relatively enriched in wheat phytoliths, and As showed the highest bio-enrichment factor between plants and phytoliths compared

with other TTMs. The results highlight the crucial role of phytoliths in alleviating TTM toxicity to wheat plant via capturing TTMs and decreasing their mobility during plant growth in heavily contaminated soil. Future research is needed to explore the mechanisms of interaction between Si and TTM ions, and to evaluate TTM sequestration capacity of phytoliths under different soil conditions by different plant species. The stability of phytoliths and potential release of TTM from phytoliths also need a clear understanding, as these factors could influence cycling of TTMs in the environment under various agricultural management practices (e.g., straw returning or burning in the field).

Acknowledgements

This research was financially supported by the Natural Science Foundation of China (Grant Nos. 41930862 and 41571130042), and State's key Project of Research and Development Plan of China (Grant Nos. 2016YFA0601002 and 2017YFC0212700).

Declaration of competing interest

The authors declare no competing interests.

References

Abbas, T., Rizwan, M., Ali, S., Adrees, M., Mahmood, A., & Zia-Ur-Rehman, M., Ibrahim, M., Arshad, M., Qayyum, M.F., 2018. Biochar application increased the growth and yield and reduced cadmium in drought stressed wheat grown in an aged contaminated soil. Ecotoxicol. Environ. Saf. 148, 825–833. https://doi.org/10.1016/j.ecoenv.2017.11.063.

Adrees, M., Ali, S., Rizwan, M., Zia-ur-Rehman, M., Ibrahim, M., Abbas, F., Farid, M., Qayyum, M.F., Irshad, M.K., 2015. Mechanisms of silicon-mediated alleviation of heavy metal toxicity in plants: A review. Ecotoxicol. Environ. Saf. 119, 186–197. https://doi.org/10.1016/j. ecoenv.2015.05.011.

Alam, M., Hussain, Z., Khan, A., Khan, M.A., Rab, A., Asif, M., Shah, M.A., Muhammad, A., 2020. The effects of organic amendments on heavy metals bioavailability in mine impacted soil and associated human health risk. Sci. Hortic-Amsterdam 262, 109067. https://doi.org/10.1016/j.scienta.2019.109067.

Ali, S., Rizwan, M., Hussain, A., Rehman, M.Z.U., Ali, B., Yousaf, B., Wijaya, L., Alyemeni, M.N., Ahmad, P., 2019. Silicon nanoparticles enhanced the growth and reduced the cadmium accumulation in grains of wheat (*Triticum aestivum* L.). Plant Physiol. Bioch. 140, 1–8. https://doi.org/10.1016/j.plaphy.2019.04.041.

Anala, R., Nambisan, P., 2015. Study of morphology and chemical composition of phytoliths on the surface of paddy straw. Paddy Water Environ. 13, 521–527. https://doi.org/10.1007/s10333-014-0468-5.

Ata-Ul-Karim, S.T., Cang, L., Wang, Y.J., Zhou, D.M., 2020. Interactions between nitrogen application and soil properties and their impacts on the transfer of cadmium from soil to wheat (*Triticum aestivum* L.) grain. Geoderma 357, 113923. https://doi.org/10.1016/j.geoderma.2019.113923.

570 Bai, J.H., Ye, X.F., Jia J.J., Zhang, G.L., Zhao, Q.Q., Cui, B.S., Liu, X.H., 2017.
571 Phosphorus sorption-desorption and effects of temperature, pH and salinity on
572 phosphorus sorption in marsh soils from coastal wetlands with different flooding
573 conditions. Chemosphere 188, 677–688.
574 https://doi.org/10.1016/j.chemosphere.2017.08.117.
575 Bao, S., 2000. Soil Agrochemical Analysis (Chinese.), China Agricultural Press,
576 Beijing.
577 Borůvka, L., Vacek, O., Jehlička, J., 2005. Principal component analysis as a tool to
578 indicate the origin of potentially toxic elements in soils. Geoderam 128, 289–300.
579 https://doi.org/10.1016/j.geoderma.2005.04.010.
580 Cai, Y.X., Zhang, S.H., Cai, K.Z., Huang, F., Pan, B.G., Wang, W., 2020. Cd
581 accumulation, biomass and yield of rice are varied with silicon application at
582 different growth phases under high concentration cadmium-contaminated soil.
583 Chemosphere 242, 125128. https://doi.org/10.1016/j.chemosphere.2019.125128.
584 Cao, Y., Dong, S., Dai, Z., Zhu, L., Xiao, T., Zhang, X., Yin, S., Soltanian, M.R.,
585 2021. Adsorption model identification for chromium (VI) transport in
586 unconsolidated sediments. J. Hydrol. 598, 126228.
587 https://doi.org/10.1016/j.jhydrol.2021.126228.
588 Castaldi, P., Silvetti, M., Manzano, R., Brundu, G., Roggero, P.P., Garau, G., 2018.
589 Mutual effect of *Phragmites australis*, *Arundo donax* and immobilization agents
590 on arsenic and trace metals phytostabilization in polluted soils. Geoderma 314,
591 63–72. https://doi.org/10.1016/j.geoderma.2017.10.040.
592 Cui, J.H., Liu, T.X., Li, F.B., Yi, J.C., Liu, C.P., Yu, H.Y., 2017. Silica nanoparticles
593 alleviate cadmium toxicity in rice cells: Mechanisms and size effects. Environ.
594 Pollut. 228, 363–369. https://doi.org/10.1016/j.envpol.2017.05.014.

595 Delplace, G., Schreck, E., Pokrovsky, O.S., Zouiten, C., Blondet, I., Darrozes, J., Viers,
596 J., 2020. Accumulation of heavy metals in phytoliths from reeds growing on
597 mining environments in Southern Europe. Sci. Total Environ. 712, 135595.
598 https://doi.org/10.1016/j.scitotenv.2019.135595.
599 Greger, M., Kabir, A.H., Landberg, T., Maity, P.J., Lindberg, S., 2016. Silicate reduces
600 cadmium uptake into cells of wheat. Environ. Pollut. 211, 90–97.
601 https://doi.org/10.1016/j.envpol.2015.12.027.
602 Guerriero, G., Stokes, I., Valle, N., Hausman, J., Exley, C., 2020. Visualising silicon in
603 plants: Histochemistry, silica sculptures and elemental imaging. Cells 9, 1066.
604 https://doi.org/10.3390/cells9041066.
605 Hogan, B., Mcdermott, F., Schmidt, O., 2018. Silicon concentrations in soil and bark
606 in Irish Sitka spruce forests. J. Plant Nutr. Soil Sci. 181, 231–239.
607 https://doi.org/10.1002/jpln.201700515.
608 Huang, H.L., Rizwan, M., Li, M., Song, F.R., Zhou, S.J., He, X., Ding, R., Dai, Z.H.,
609 Yuan, Y., Cao, M.H., Xiong, S.L., Tu, S.X., 2019. Comparative efficacy of
610 organic and inorganic silicon fertilizers on antioxidant response, Cd/Pb
611 accumulation and health risk assessment in wheat (*Triticum aestivum* L.).
612 Environ. Pollut. 255, 113146. https://doi.org/10.1016/j.envpol.2019.113146.
613 Imtiaz, M., Rizwan, M.S., Mushtaq, M.A., Ashraf, M., Shahzad, S.M., Yousaf, B.,
614 Saeed, D.A., Rizwan, M., Nawaz, M.A., Mehmood, S., Tu, S.X., 2016. Silicon
615 occurrence, uptake, transport and mechanisms of heavy metals, minerals and
616 salinity enhanced tolerance in plants with future prospects: A review. J. Environ.
617 Manage. 183, 521–529. https://doi.org/10.1016/j.jenvman.2016.09.009.
618 Khan, Z.S., Rizwan, M., Hafeez, M., Ali, S., Adrees, M., Qayyum, M.F., Khalid, S.,
619 Rehman, M.Z.U., Sarwar, M.A., 2020. Effects of silicon nanoparticles on growth

620 and physiology of wheat in cadmium contaminated soil under different soil
621 moisture levels. Environ. Sci. Pollut. Res. 27, 4958–4968.
622 https://doi.org/10.1007/s11356-019-06673-y.
623 Li, J., Zheng, L., Wang, S.L., Wu, Z., Wu, W., Niazi, N.K., Shaheen, S.M., Rinklebe,
624 J., Bolan, N., Ok, Y.S., Wang, H., 2019. Sorption mechanisms of lead on
625 silicon-rich biochar in aqueous solution: Spectroscopic investigation. Sci. Total
626 Environ. 672, 572–582. https://doi.org/10.1016/j.scitotenv.2019.04.003.
627 Li, R.C., Fan, J., Carter, J., Jiang, N., and Gu, Y.S., 2017. Monthly variations of
628 phytoliths in the leaves of the bamboo *Dendrocalamus ronganensis* (Poaceae:
629 Bambusoideae). Rev. Palaeobot. Palyno. 246, 62–69.
630 http://dx.doi.org/10.1016/j.revpalbo.2017.06.006.
631 Li, Y.P., Zhang, Y.Q., Ippolito, J.A., Xing, W.Q., Qiu, K.Y., Yang, H., 2020. Lead
632 smelting effects heavy metal concentrations in soils, wheat, and potentially
633 humans. Environ. Pollut. 257, 113641.
634 https://doi.org/10.1016/j.envpol.2019.113641.
635 Li, Z.M., Song, Z.L., Parr, J.F., Wang, H.L., 2013. Occluded C in rice phytoliths:
636 implications to biogeochemical carbon sequestration. Plant Soil 370, 615–623.
637 https://doi.org/10.1007/s11104-013-1661-9.
638 Li, Z.M., Song, Z.L., Cornelis, J.T., 2014. Impact of rice cultivar and organ on
639 elemental composition of phytoliths and the release of bio-available silicon.
640 Front. Plant Sci. 5, 529. https://doi.org/10.3389/fpls.2014.00529.
641 Li, Z., Delvaux, B.,2019. Phytolith-rich biochar: A potential Si fertilizer in desilicated
642 soils. GCB Bioenergy 11, 1264–1282. https://doi.org/10.1111/gcbb.12635.
643 Liang, Y.C., Wong, J.W.C., Wei, L., 2005. Silicon-mediated enhancement of cadmium
644 tolerance in maize (*Zea mays* L.) grown in cadmium contaminated soil.

Chemosphere 58, 475–483. https://doi.org/10.1016/j.chemosphere.2004.09.034.

Liu, J., Ma, J., He, C., Li, X., Zhang, W., Xu, F., Lin, Y., Wang, L., 2013. Inhibition of cadmium ion uptake in rice (*Oryza sativa*) cells by a wall-bound form of silicon. New Phytol. 200, 691–699. https://doi.org/10.1111/nph.12494.

Liu, L.N., Song, Z.L., Yu, C.X., Yu, G.H., Ellam, R.M., Liu, H.Y., Singh, B.P., Wang, H.L., 2020a. Silicon effects on biomass carbon and phytolith-occluded carbon in grasslands under high-salinity conditions. Front. Plant Sci. 11, 657. https://doi.org/10.3389/fpls.2020.00657.

Liu, X.X., Yin, L.N., Deng, X.P., Gong, D., Du, S., Wang, S.W., Zhang, Z.Y., 2020b. Combined application of silicon and nitric oxide jointly alleviated cadmium accumulation and toxicity in maize. J. Hazard. Mater. 395, 122679. https://doi.org/10.1016/j.jhazmat.2020.122679.

Loganathan, P., Vigneswaran, S., Kandasamy, J., Naidu, R., 2012. Cadmium sorption and desorption in soils: a review. Critical Rev. Environ. Sci. Technol. 42, 489–533. https://doi.org/10.1080/10643389.2010.520234.

Lu, R., 2000. Methods of Soil and Agrochemical Analysis (in Chinese). China Agricultural Science and Technology Press, Beijing.

Ma, J., Cai, H., He, C., Zhang, W., Wang, L., 2015. A hemicellulose-bound form of silicon inhibits cadmium ion uptake in rice (*Oryza sativa*) cells. New Phytol. 206, 1063-1074. https://doi.org/10.1111/nph.13276.

Ma, J.F., 2010. Silicon transporters in higher plants, in: Jahn, T.P., Bienert, G.P. (Eds.), MIPs and Their Role in the Exchange of Metalloids. Springer, New York, NY, USA, pp. 99–109.

Ma, J.F., Yamaji, N., 2008. Functions and transport of silicon in plants. Cell. Mol. Life Sci. 65, 3049–3057. https://doi.org/10.1007/s00018-008-7580-x.

Ma, J., Zhang, X.Q., Wang, L.J., 2017. Synergistic effects between [Si-hemicellulose matrix] ligands and Zn ions in inhibiting Cd ion uptake in rice (*Oryza sativa*) cells. Planta 245, 965. https://doi.org/10.1007/s00425-017-2655-2.

Mao, C., Song, Y., Chen, L., Ji, J., Li, J., Yuan, X., Yang, Z., Ayoko, G.A., Frost, R.L., Theiss, F., 2019. Human health risks of heavy metals in paddy rice based on transfer characteristics of heavy metals from soil to rice. CATENA 175, 339–348. https://doi.org/10.1016/j.catena.2018.12.029.

Meharg, C., Meharg, A.A., 2015. Silicon, the silver bullet for mitigating biotic and abiotic stress, and improving grain quality, in rice? Environ. Exp. Bot. 120, 8–17. https://doi.org/10.1016/j.envexpbot.2015.07.001.

Murtaza, B., Naeem, F., Shahid, M., Abbas, G., Shah, N.S., Amjad, M., Bakhat, H.F., Imran, M., Niazi, N.K., Murtaza, G., 2019. A multivariate analysis of physiological and antioxidant responses and health hazards of wheat under cadmium and lead stress. Environ. Sci. Pollut. Res. 26, 362–370. https://doi.org/10.1007/s11356-018-3605-7.

Nawaz, M.A., Zakharenko, A.M., Zemchenko, I.V., Haider, M.S., Ali, M.A., Imtiaz, M., Chung, G., Tsatsakis, A., Sun, S., Golokhvast, K.S., 2019. Phytolith Formation in Plants: From Soil to Cell. Plants 8, 249. https://doi.org/10.3390/plants8080249.

Neu, S., Schaller, J., and Gert, D.E., 2017. Silicon availability modifies nutrient use efficiency and content, C:N:P stoichiometry, and productivity of winter wheat (*Tritium astivum* L.). Sci. Rep. 7, 40829. https://doi.org/10.1038/srep40829.

Nguyen, T.N., Nguyen, M.N., McNamara, M., Dultz, S., Meharg, A., Nguyen, V.T., 2019. Encapsulation of lead in rice phytoliths as a possible pollutant source in paddy soils. Environ. Exp. Bot. 162, 58–66.

https://doi.org/10.1016/j.envexpbot.2019.02.009.

Nguyen, M.N., Dam, A.T.Q., Nguyen, A.M., Nguyen, L.N., Duong, L.T., Dang, Q.T., Tran, T.T., 2021. Arsenic in rice straw phytoliths: Encapsulation and release properties. Applied Geochemistry 127, 104907. https://doi.org/10.1016/j.apgeochem.2021.104907.

Pan, D., 2014. The impact of agricultural extension on farmer nutrient management behavior in Chinese rice production: A Household-Level Analysis. Sustainability, 6, 6644-6665. https://doi.org/10.3390/su6106644.

Paolicchi, M., Benvenuto, M.L., Honaine, M.F., Osterrieth, M., 2019. Root silicification of grasses and crops from the Pampean region and its relevance to silica and silicophytolith content of soils. Plant Soil 444, 351–363. https://doi.org/10.1007/s11104-019-04287-4.

Parr, J.F., Sullivan, L.A., 2011. Phytolith occluded carbon and silica variability in wheat cultivars. Plant Soil 342, 165–171. https://doi.org/10.1007/s11104-010-0680-z.

Puppe, D., Sommer, M., 2018. Experiments, uptake mechanisms, and functioning of silicon foliar fertilizationd - A review focusing on maize, rice, and wheat. Adv. Agron. 152, 1–49. https://doi.org/10.1016/bs.agron.2018.07.003.

Qi, L.M., Li, F.Y., Huang, Z.T., Jiang, P.K., Baoyin, T., Wang, H.L., 2017. Phytolith-occluded organic carbon as a mechanismfor long-termcarbon sequestration in a typical steppe: The predominant role of belowground productivity. Sci. Total Environ. 577, 413–417. http://dx.doi.org/10.1016/j.scitotenv.2016.10.206.

Rizwan, M., Meunier, J.D., H_el_ene, M., Keller, C., 2012. Effect of silicon on reducing cadmium toxicity in durum wheat (*Triticum turgidum* L. cv. Claudio

720 W.) grown in a soil with aged contamination. J. Hazard Mater. 209–210,
721 326–334. https://doi.org/10.1016/j.jhazmat.2012.01.033
722 Rogalla, H., Römheld, V., 2002. Role of leaf apoplast in silicon-mediated manganese
723 tolerance of *Cucumis sativus* L. Plant Cell Environ. 25, 549–555.
724 https://doi.org/10.1046/j.1365-3040.2002.00835.x
725 Safari, Y., Delavar, M.A., Zhang, C., Noori, Z., Rahmanian, M., 2018. Assessing
726 cadmium risk in wheat grain using soil threshold values. Int. J. Environ. Sci.
727 Technol. 15, 887–894. https://doi.org/10.1007/s13762-017-1422-z.
728 Schaller, J., Brackhage, C., and Dudel, E.G., 2012. Silicon availability changes
729 structural carbon ratio and phenol content of grasses. Environ. Exp. Bot. 77,
730 283–287. https://doi.org/10.1016/j.envexpbot.2011.12.009.
731 Soltanian, M.R., Ritzi, R.W., Huang, C.C., Dai, Z., 2015. Relating reactive solute
732 transport to hierarchical and multiscale sedimentary architecture in a
733 Lagrangian-based transport model: 1. Time-dependent effective retardation factor.
734 Water Resour. Res. 51,1586–1600. https://doi.org/10.1002/2014WR016353.
735 Song, Z.L., Liu, H.Y., Li, B.L., Yang, X.M., 2013. The production of
736 phytolith-occluded carbon in China's forests: implications to biogeochemical
737 carbon sequestration. Global Change Biol. 19, 2907–2915.
738 https://doi.org/10.1111/gcb.12275.
739 Song, Z.L., Müller, K., Wang, H.L., 2014. Biogeochemical silicon cycle and carbon
740 sequestration in agricultural ecosystems. Earth-Sci. Rev. 139, 268–278.
741 http://dx.doi.org/10.1016/j.earscirev.2014.09.009.
742 Song, Z.L., McGrouther, K., Wang, H.L., 2016. Occurrence, turnover and carbon
743 sequestration potential of phytoliths in terrestrial ecosystems. Earth-Sci. Rev.
744 158, 19–30. http://dx.doi.org/10.1016/j.earscirev.2016.04.007.

745 Tan, X., Wang, Z., Liu, M., He, K., 2020. Determination of trace metals in garlic
746 bulbs (*Allium sativum* L.): A variety discrimination by inductively coupled
747 plasma mass spectrometry. J. Appl. Spectrosc. 87, 194–199.
748 http://dx.doi.org/10.1007/s10812-020-00982-8.
749 Tran, T.T.T., Nguyen, T.T., Nguyen, V.T., Huynh, H.T.H., Nguyen, T.T.H., Nguyen,
750 M.N., 2019. Copper encapsulated in grass-derived phytoliths: Characterization,
751 dissolution properties and the relation of content to soil properties. J. Environ.
752 Manage. 249, 109423. https://doi.org/10.1016/j.jenvman.2019.109423.
753 Trinh, T.K., Nguyen, T.T.H., Nguyen, T.N., Wu, T.Y., Meharg, A.A., Nguyen, M.N.,
754 2017. Characterization and dissolution properties of phytolith occluded
755 phosphorus in rice straw. Soil Till. Res. 171, 19–24.
756 http://dx.doi.org/10.1016/j.still.2017.04.002.
757 Walkley, A., Black, I.A., 1934. Estimation of soil organic carbon by the chromic acid
758 titration method. Soil Sci. 37, 29–38.
759 https://doi.org/10.1097/00010694-193401000-00003.
760 Wang, H., Wang, X., Peng, B., 2021. Using an improved Si-rich husk ash to decrease
761 inorganic arsenic in rice grain. Sci. Total Environ. 803, 150102.
762 https://doi.org/10.1016/j.scitotenv.2021.150102.
763 Wang, M.S., Han,Q., Gui, C.L., Cao, J.L., Liu, Y.P., He, X.D., He, Y.C., 2019a.
764 Differences in the risk assessment of soil heavy metals between newly built and
765 original parks in Jiaozuo, Henan Province, China. Sci. Total Environ. 676, 1–10.
766 https://doi.org/10.1016/j.scitotenv.2019.03.396.
767 Wang, S., Wang, F., Gao, S., Wang, X., 2016. Heavy metal accumulation in different
768 rice cultivars as influenced by foliar application of nano-silicon. Water Air Soil
769 Pollut. 227, 1–13. https://doi.org/10.1007/s11270-016-2928-6

770 Wang, Y.Y., Li, F.F., Wang, X.Y., Yang, Z.H., Han, K., Ruan, X.L., 2019b. Spatial
771 distribution and risk assessment of heavy metal contamination in surface
772 farmland soil around a lead and zinc smelter. Environ. Sci. 40, 437–444.
773 https://doi.org/10.13227 /j.hjkx.201803031.
774 Wang, Y.Y., Liu, Y.D., Zhan, W.H., Zheng, K.X., Wang, J.N., Zhang, C.S., Chen, R.H.,
775 2020a. Stabilization of heavy metal-contaminated soils by biochar: challenges
776 and recommendations. Sci. Total Environ. 729, 139060.
777 https://doi.org/10.1016/j.scitotenv.2020.139060.
778 Wang, Y.Y., Liu, Y.D., Zhan, W.H., Zheng, K.X., Lian, M.M., Zhang, C.S., Ruan, X.L.,
779 Li, T., 2020b. Long-term stabilization of Cd in agricultural soil using
780 mercapto-functionalized nano-silica (MPTS/nano-silica): A three-year field study.
781 Ecotox. Environ. Safe. 197, 110600.
782 https://doi.org/10.1016/j.ecoenv.2020.110600.
783 Wüst, R.A.J., Bustin, R., 2003. Opaline and Al–Si phytoliths from a tropical mire
784 system of West Malaysia: abundance, habit, elemental composition, preservation
785 and significance. Chem. Geol. 200, 267–292.
786 https://doi.org/10.1016/S0009-2541(03)00196-7.
787 Xue, P.Y., Zhao,Q.L., Sun, H.X., Geng, L.P., Yang, Z.Z., Liu, W.J., 2019.
788 Characteristics of heavy metals in soils and grains of wheat and maize from
789 farmland irrigated with sewage. Environ. Sci. Pollut. Res. 26, 5554–5563.
790 https://doi.org/10.1007/s11356-018-3997-4.
791 Yang, W.X., Wang, D., Wang, M.K., Zhou F., Huang J., Xue, M.Y., Dinh, Q.T.,
792 Liang, D.L., 2019. Heavy metals and associated health risk of wheat grain in a
793 traditional cultivation area of Baoji, Shaanxi, China. Environ. Monit. Assess. 191,
794 428. https://doi.org/10.1007/s10661-019-7534-9.

795 Yin, D., Wang, X., Chen, C., Peng, B., Tan, C., Li, H., 2016. Varying effect of
796 biochar on Cd, Pb and As mobility in a multi-metal contaminated paddy soil.
797 Chemosphere 152, 196–206. https://doi.org/10.1016/j.chemosphere.2016.01.044.
798 Zhang, X.D., Song, Z.L., Hao, Q., Yu, C.X., Liu, H.Y., Chen, C.M., Müller, K., Wang,
799 H.L., 2020. Storage of soil phytoliths and phytolith-occluded carbon along a
800 precipitation gradient in grasslands of northern China. Geoderma 364, 114200.
801 https://doi.org/10.1016/j.geoderma.2020.114200.
802 Zhao, Q., Zeng, D.H., 2019. Nitrogen addition effects on tree growth and soil
803 properties mediated by soil phosphorus availability and tree species identity. For.
804 Ecol. Manag. 449, 117478. https://doi.org/10.1016/j.foreco.2019.117478.
805 Zheng, S.N., Wang, Q., Yu, H.Y., Huang, X.Z., Li, F.B., 2020. Interactive effects of
806 multiple heavy metal(loid)s on their bioavailability in cocontaminated paddy
807 soils in a large region. Sci. Total Environ. 708, 135126.
808 https://doi.org/10.1016/j.scitotenv.2019.135126.
809 Zhou, H.M., Wang, P., Chen, D., Shi, G.L., Cheng, K., Bian, R.J., Liu, X.Y., Zhang,
810 X.H., Zheng, J.F., Crowley, D.E., Zwieten, L.V., Li, L.Q., Pan, G.X., 2018.
811 Short-term biochar manipulation of microbial nitrogen transformation in wheat
812 rhizosphere of a metal contaminated Inceptisol from North China plain. Sci.
813 Total Environ. 640–641, 1287–1296.
814 https://doi.org/10.1016/j.scitotenv.2018.06.009.
815

Tables:

Table 1 Physicochemical properties of multi-element contaminated soil under lightly and heavily polluted conditions.

Properties	Units	Light pollution (LP)	Heavy pollution (HP)	Sig.
pH		7.72 ± 0.08	7.42 ± 0.02	**
Electrical conductivity	mS m^{-1}	35.2 ± 7.70	44.8 ± 18.6	–
Water content	%	16.1 ± 3.32	14.0 ± 1.57	–
Bulk density	g cm^{-3}	2.34 ± 0.18	2.54 ± 0.28	–
Organic C	%	1.86 ± 0.22	1.55 ± 0.23	**
Clay	%	8.11 ± 0.27	7.63 ± 0.33	**
Silt	%	76.3 ± 2.70	73.6 ± 2.06	*
Sand	%	12.3 ± 3.14	15.6 ± 2.67	**
Available N	mg g^{-1}	0.08 ± 0.01	0.08 ± 0.01	–
Available P	mg g^{-1}	0.06 ± 0.02	0.05 ± 0.01	–
Available Si	mg g^{-1}	0.24 ± 0.02	0.20 ± 0.01	**
Total TTMs				
Pb	mg g^{-1}	0.43 ± 0.11	1.13 ± 0.59	**
Zn	mg g^{-1}	0.14 ± 0.02	0.25 ± 0.09	**
Cd	mg g^{-1}	0.01 ± 0.00	0.04 ± 0.02	**
Cu	mg g^{-1}	0.05 ± 0.01	0.06 ± 0.01	*
As	mg g^{-1}	0.03 ± 0.01	0.05 ± 0.01	**
Available TTMs				
Pb	μg g^{-1}	0.02 ± 0.02	0.11 ± 0.10	**
Zn	μg g^{-1}	0.05 ± 0.04	0.18 ± 0.11	**
Cd	μg g^{-1}	0.23 ± 0.08	1.32 ± 1.08	**
Cu	μg g^{-1}	0.14 ± 0.04	0.18 ± 0.02	**
As	μg g^{-1}	0.59 ± 0.22	0.72 ± 0.17	–

Note: Values are means ± SD (n = 12). * and ** represent significant difference between different pollution conditions at $p < 0.05$ and $p < 0.01$ level, respectively; – represent the correlation being not significant.

824 **Table 2** Contents of Si and phytoliths in different wheat tissues under lightly and heavily polluted

825 soil conditions.

Content (%)	Light pollution (LP)			Heavy pollution (HP)		
	Leaf sheath	Culm	Inflorescence	Leaf sheath	Culm	Inflorescence
Silicon	4.12 ± 0.74^{bA}	1.68 ± 0.27^{cA}	4.88 ± 0.58^{aA}	3.74 ± 0.63^{bA}	1.61 ± 0.32^{cA}	4.56 ± 0.61^{aA}
Phytoliths	9.95 ± 1.39^{bA}	3.80 ± 0.59^{cA}	11.2 ± 1.28^{aA}	9.03 ± 1.61^{aA}	3.58 ± 0.83^{bA}	9.81 ± 1.58^{aB}

826 Notes: Lowercase (a, b and c) represent significant differences between different wheat tissues;

827 capital letters (A and B) represent significant differences between different pollution conditions (p

828 < 0.05, $n = 12$).

829

Table 3 Pearson correlation coefficients between the contents of plant TTMs and PhytTMs in different wheat tissues under lightly and heavily polluted soil conditions, at $^{**}p < 0.01$ and $^{*}p < 0.05$ level.

	Light pollution			Heavy pollution		
	Leaf sheath	**Culm**	**Inflorescence**	**Leaf sheath**	**Culm**	**Inflorescence**
Pb	0.791**	-0.014	0.318	0.931**	0.888**	0.913**
Zn	0.547	0.666*	-0.365	0.904**	0.704*	0.856**
Cd	0.546	0.380	0.063	0.719**	0.790**	0.830**
Cu	0.420	0.479	0.191	0.895**	0.861**	0.880**
As	0.781**	0.596**	0.368	0.764**	0.555	0.564

Figure legends:

Fig. 1 Various morphologies of the phytoliths extracted from wheat tissues characterized by field-emission scanning electron microscope (FE-SEM); A-L are the nano-scale structures of the phytoliths in the subplots (a-l), which are the morphologies of the phytoliths extracted from inflorescences (a-d), leaf sheaths (e-h) and culms (i-l), respectively.

Fig. 2 Toxic trace metal(loid) contents in plant tissues (a – c) and phytoliths (d – f) of wheat under lightly (LPs) and heavily (HPs) polluted soil conditions. * and ** represent significant differences between different pollution conditions at $p < 0.05$ and $p < 0.01$ level, respectively.

Fig. 3 Enrichment factors of TTMs between plants and soils (a-c), and phytoliths and plants (d-f) under lightly (LPs) and heavily (HPs) polluted soil conditions. Different letters over boxes represent significant differences between LPs and HPs at level $p < 0.05$. Dots outside the bars and asterisks inside the bars represent outliers and mean values, respectively.

Fig. 4 Principle components analysis (PCA) of soil physico-chemical properties [i.e., water content (WC), pH value, bulk density (BD), electrical conductivity (EC) and particle size (i.e., clay, silt and sand)], nutrient elements [i.e., soil organic carbon (SOC), available nitrogen (AN), available phosphorus (AP) and available silicon (ASi)], and TTMs [i.e., total Pb, Zn, Cu, Cd and As, and available elements (APb, AZn, ACu, ACd and AAs)] in lightly (LPs) (yellow dots) and heavily (HPs) (blue dots) polluted soils.

Fig. 5 Network visualization of the correlations between soil (blue) elements [i.e., available elements (denoted by A+element) and organic carbon (SOC)], and plant (yellow) elements and PhytTMs (red) (denoted by P+element) in wheat tissues under lightly (LPs) and heavily (HPs) polluted soil conditions. Non-significant correlations are displayed outside the network. Solid and dotted lines indicate positive and negative correlations, respectively. All lines indicate significance at $p < 0.05$ level, and thicker lines represent stronger correlations.

Figures:

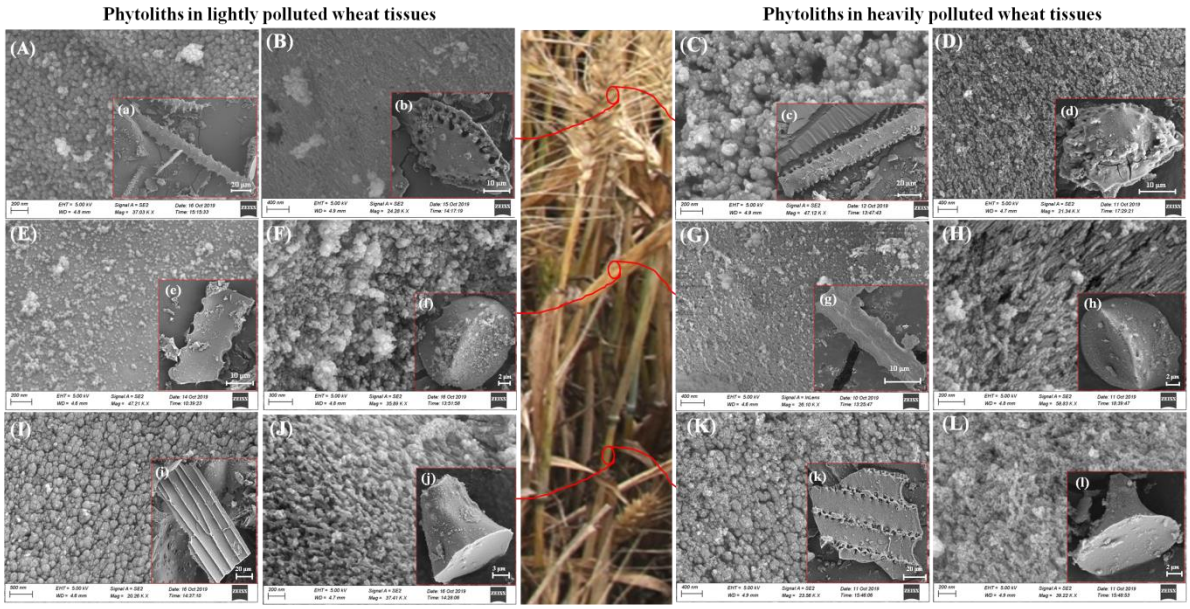

Fig. 1 Various morphologies of the phytoliths extracted from wheat tissues characterized by field-emission scanning electron microscope (FE-SEM); A-L are the nano-scale structures of the phytoliths in the subplots (a-l), which are the morphologies of the phytoliths extracted from inflorescences (a-d), leaf sheaths (e-h) and culms (i-l), respectively.

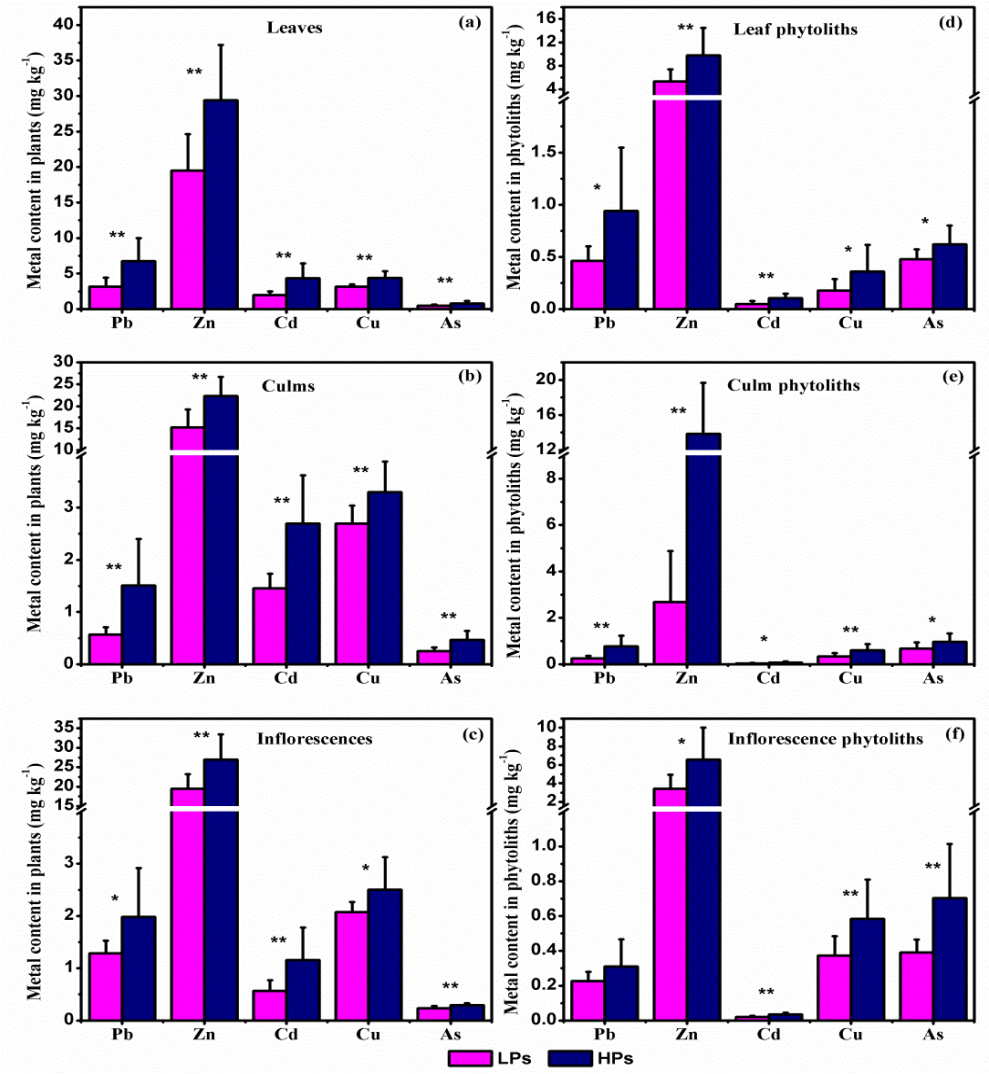

870

871 **Fig. 2** Toxic trace metal(loid) contents in plant tissues (a – c) and phytoliths (d – f) of wheat under

872 lightly (LPs) and heavily (HPs) polluted soil conditions. * and ** represent significant differences

873 between different pollution conditions at $p < 0.05$ and $p < 0.01$ level, respectively.

874

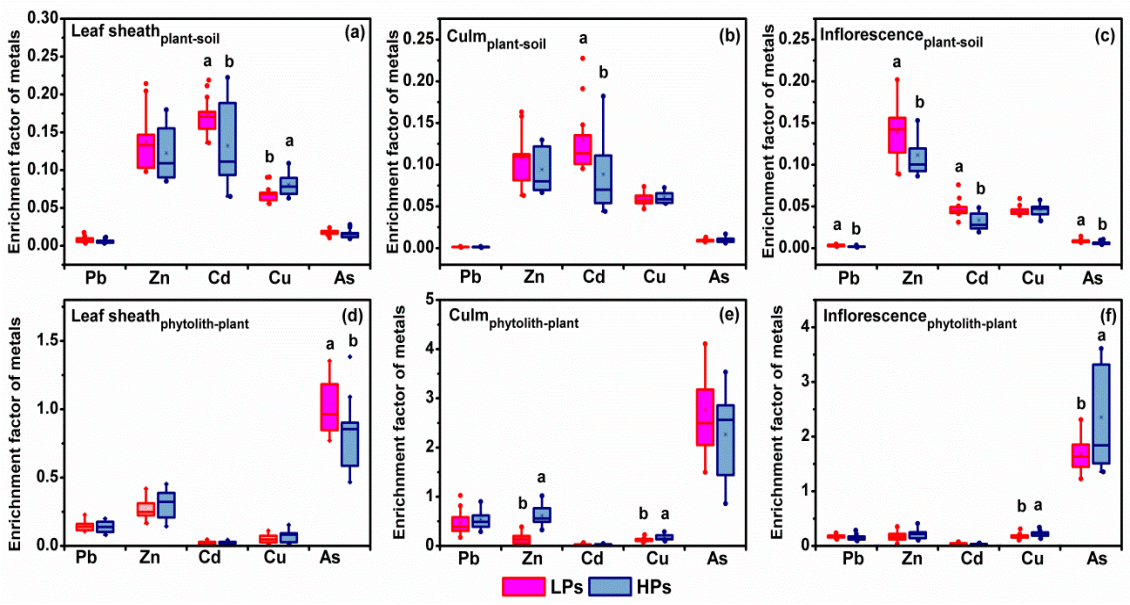

875

876 **Fig. 3** Enrichment factors of TTMs between plants and soils (a-c), and phytoliths and plants (d-f)

877 under lightly (LPs) and heavily (HPs) polluted soil conditions. Different letters over boxes

878 represent significant differences between LPs and HPs at level $p < 0.05$. Dots outside the bars and

879 asterisks inside the bars represent outliers and mean values, respectively.

880

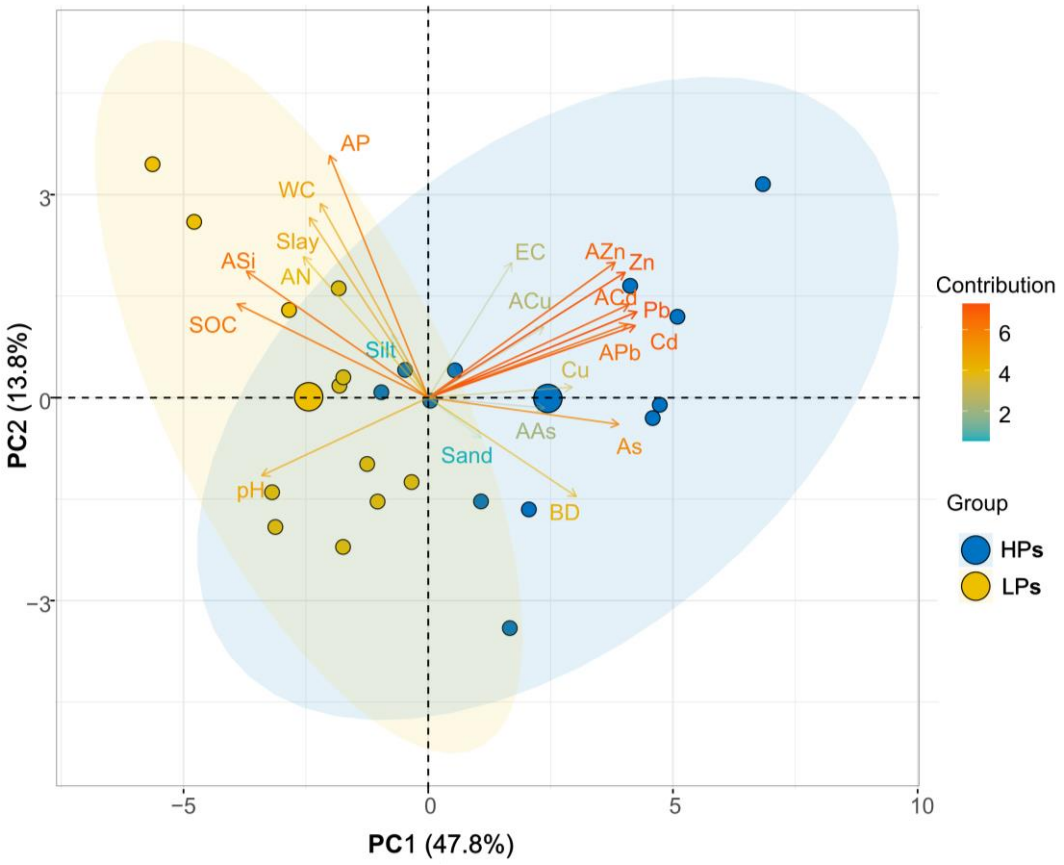

Fig. 4 Principle components analysis (PCA) of soil physico-chemical properties [i.e., water content (WC), pH value, bulk density (BD), electrical conductivity (EC) and particle size (i.e., clay, silt and sand)], nutrient elements [i.e., soil organic carbon (SOC), available nitrogen (AN), available phosphorus (AP) and available silicon (ASi)], and TTMs [i.e., total Pb, Zn, Cu, Cd and As, and available elements (APb, AZn, ACu, ACd and AAs)] in lightly (LPs) (yellow dots) and heavily (HPs) (blue dots) polluted soils.

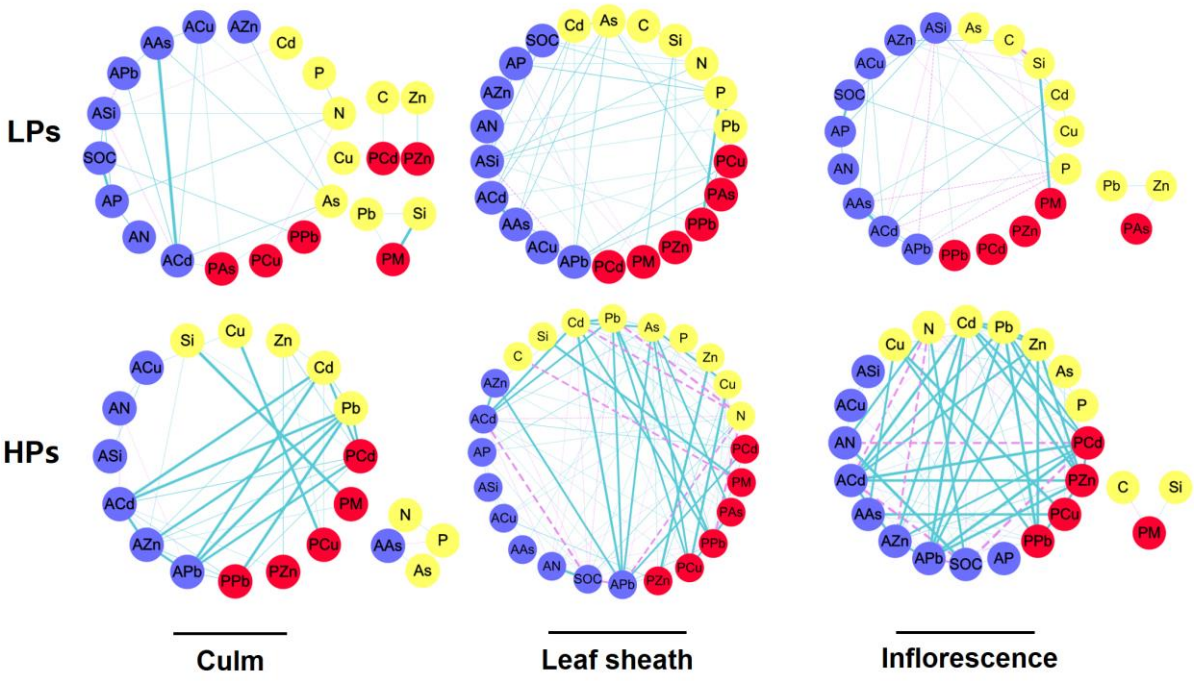

Fig. 5 Network visualization of the correlations between soil (blue) elements [i.e., available elements (denoted by A+element) and organic carbon (SOC)], and plant (yellow) elements and PhytTMs (red) (denoted by P+element) in wheat tissues under lightly (LPs) and heavily (HPs) polluted soil conditions. Non-significant correlations are displayed outside the network. Solid and dotted lines indicate positive and negative correlations, respectively. All lines indicate significance at $p < 0.05$ level, and thicker lines represent stronger correlations.

Supplementary Information

Table S1. Contents of TTMs in plant tissues and phytoliths, and PhytTMs in different tissues of wheat under lightly and heavily polluted conditions.

		Light pollution			Heavy pollution		
		Leaf sheath	Culm	Inflorescence	Leaf sheath	Culm	Inflorescence
In plants (mg kg^{-1})	Pb	3.18±1.26^{a}	0.57±0.14^{c}	1.29±0.24^{b}	6.75±3.24^{a}	1.51±0.89^{b}	1.98±0.93^{b}
	Zn	19.5±5.13^{a}	15.2±4.06^{b}	19.5±3.73^{a}	29.4±7.77^{a}	22.3±4.37^{b}	27.0±6.46^{ab}
	Cd	2.00±0.51^{a}	1.45±0.28^{b}	0.57±0.20^{c}	4.33±2.11^{a}	2.70±0.92^{b}	1.56±0.62^{c}
	Cu	3.16±0.33^{a}	2.70±0.34^{b}	2.07±0.20^{c}	4.37±0.99^{a}	3.30±0.58^{b}	2.50±0.62^{c}
	As	0.48±0.15^{a}	0.25±0.07^{b}	0.23±0.04^{b}	0.81±0.35^{a}	0.47±0.17^{b}	0.29±0.04^{b}
In phytoliths (mg kg^{-1})	Pb	0.46±0.14^{a}	0.26±0.11^{b}	0.23±0.06^{b}	0.94±0.61^{a}	0.77±0.46^{a}	0.31±0.16^{b}
	Zn	5.31±2.10^{a}	2.68±2.19^{b}	3.40±1.53^{b}	9.79±4.67^{b}	13.9±5.81^{a}	6.55±3.46^{b}
	Cd	0.05±0.03^{a}	0.04±0.02^{a}	0.02±0.01^{b}	0.10±0.04^{a}	0.07±0.04^{b}	0.03±0.01^{c}
	Cu	0.18±0.11^{b}	0.34±0.14^{a}	0.37±0.11^{a}	0.36±0.25^{b}	0.60±0.27^{a}	0.58±0.22^{a}
	As	0.48±0.67^{b}	0.67±0.26^{a}	0.39±0.07^{b}	0.62±0.18^{b}	0.96±0.36^{a}	0.70±0.31^{b}
PhytTMs (mg kg^{-1})	Pb	0.05±0.01^{a}	0.01±0.00^{c}	0.03±0.01^{b}	0.08±0.05^{a}	0.03±0.02^{b}	0.03±0.01^{b}
	Zn	0.54±0.26^{a}	0.10±0.10^{c}	0.38±0.16^{b}	0.90±0.41^{a}	0.49±0.24^{b}	0.63±0.32^{ab}
	Cd	<0.01^{a}	<0.01^{b}	<0.01^{b}	0.01±0.00^{a}	<0.01^{b}	<0.01^{b}
	Cu	0.02±0.01^{b}	0.01±0.00^{b}	0.04±0.01^{a}	0.03±0.02^{b}	0.02±0.01^{b}	0.06±0.02^{a}
	As	0.05±0.01^{a}	0.02±0.01^{b}	0.04±0.01^{a}	0.05±0.01^{a}	0.04±0.01^{b}	0.07±0.03^{a}

Note: Different letters in superscript represent significant differences between wheat tissues at $p < 0.05$ level according to One-Way ANOVA.

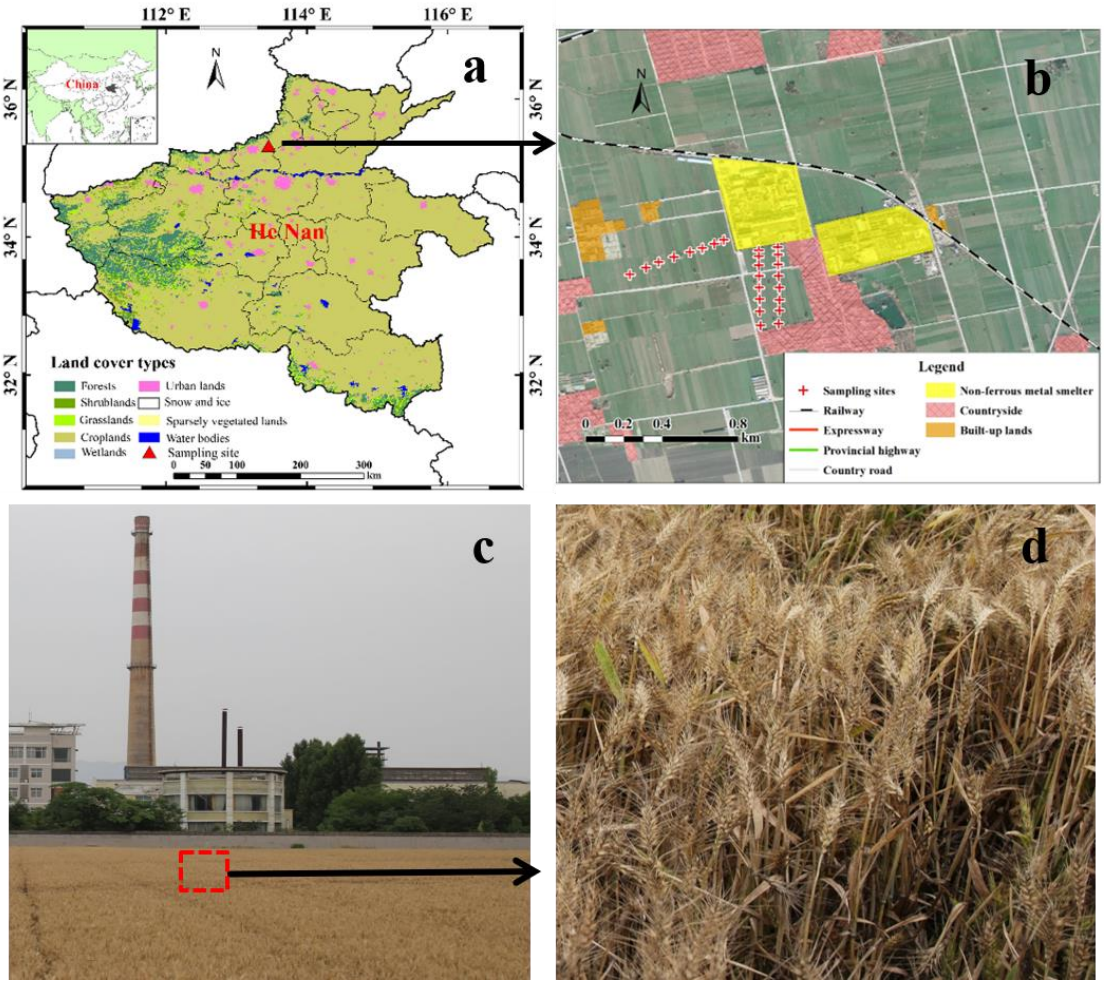

Fig. S1 Location of the sampling sites around the Pb/Zn smelter in Henan Province, China. The red triangle in figure (a) is the location of the smelter, and the red stars in figure (b) are the distribution of sampling sites around the smelter. Figure (c) represents one of the sampling sites, and figure (d) shows the standing wheat crops contaminated by the discharged wastewater and gas from the nearby smelter.

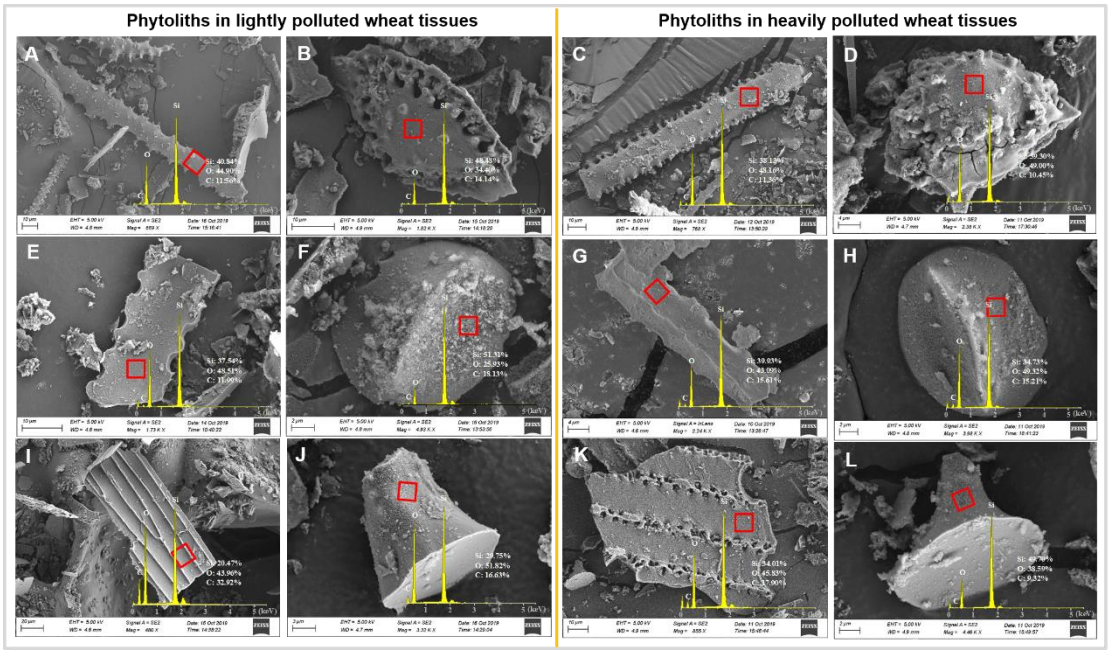

Fig. S2 Various morphologies (A-L) of the phytoliths extracted from wheat tissues characterized by field-emission scanning electron microscope (FE-SEM) and the mass percent of Si, O and C assessed by EDS spectra on the corresponding phytoliths obtained at the region of red rectangle.

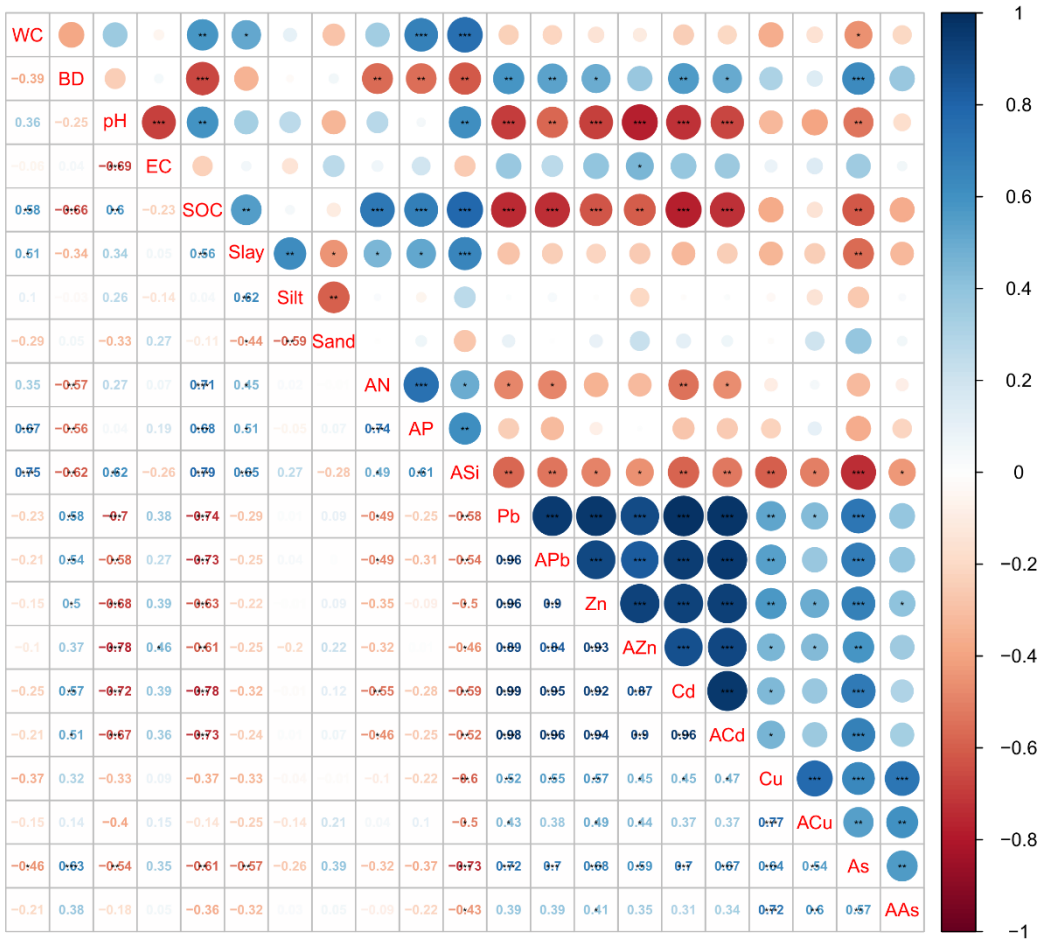

Fig. S3 Correlation coefficients between soil texture, nutrient and TTM contents in soils. *, ** and *** represent the significant differences at $p < 0.05$, $p < 0.01$ and $p < 0.001$ level, respectively. A+element represents available element.